

## Muon magnetic anomaly: experimental status and prospects

Dinko Počanić

*Department of Physics, University of Virginia, Charlottesville, VA 22904-4714, USA*



The past five years have brought significant new results on the muon magnetic anomaly,  $a_\mu = (g_\mu - 2)/2$ , and on the hadronic vacuum polarization (HVP) contribution dominating the uncertainty  $\Delta a_\mu$ . Serious tension has emerged between the experimental and standard model (SM) values for  $a_\mu$ , as well as between the SM and the first precise lattice QCD values. We review the current experimental and theoretical status of  $a_\mu$ , along with the prospects for new results, focusing on MUonE, a new experiment at CERN, aiming to evaluate the leading order contribution to  $a_\mu^{\text{HVP}}$  in a direct measurement of muonic Bhabha scattering.

### 1 The physics of the muon magnetic anomaly

The magnetic moments of the electron and muon, given by their gyromagnetic ratios  $g_{e,\mu}$ ,

$$\vec{\mu}_\ell = g_\ell \left( \frac{q}{2m_\ell} \right) \vec{S}, \quad \text{where} \quad g_\ell = 2(1 + a_\ell), \quad \text{and} \quad \ell = e, \mu,$$

have played an important role in the development of the standard model (SM). The Dirac theory<sup>1</sup> predicted that  $g_e = 2$ , resolving a decades-long search for a fundamental explanation of this anomaly. About 20 years later, Schwinger<sup>2</sup> proposed an additional contribution to  $\mu_e$  from a radiative correction, predicting the anomaly<sup>a</sup>  $a_e = \alpha/2\pi \simeq 0.00116$  in good agreement with contemporary experiments.<sup>3</sup> A decade later, a precise experiment<sup>4</sup> confirmed Schwinger's prediction for the muon anomaly, and thereby established for the first time that, in a magnetic field, a muon behaves simply like a massive electron, which, in turn, paved the way for the notion of lepton generations.

In the SM, the muon anomaly receives contributions from electromagnetic, strong and weak interactions that arise from virtual effects involving photons, leptons, hadrons, as well as the  $W$ ,  $Z$ , and Higgs bosons,<sup>5</sup> as shown in Fig. 1. While  $a_e$ , the electron magnetic anomaly, is experimentally determined far more precisely than  $a_\mu$ , the latter is  $(m_\mu/m_e)^2 \simeq 43,000$  times more sensitive to contributions from heavy additions to the SM through processes similar to those illustrated in Fig. 1. This extraordinary sensitivity has motivated the international theory

<sup>a</sup>The quantity  $a_\ell$  is the magnetic anomaly, but is also often referred to simply as the “anomaly” or as the “anomalous magnetic moment”.

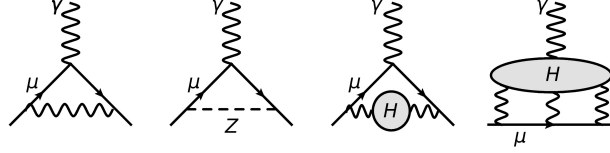


Figure 1 – Feynman diagrams of representative SM contributions to  $a_\mu$ . From left to right: first-order QED and weak processes, leading-order hadronic (H) vacuum polarization and hadronic light-by-light contributions.

community to embark on a comprehensive program of evaluating  $a_\mu$  that culminated in the 2020 prediction of  $a_\mu(\text{SM}) = 116\,591\,810(43) \times 10^{-11}$  (0.37 ppm), based on calculations of previously unparalleled precision, published in the 2020 Muon  $g-2$  Theory Initiative White Paper (TIWP).<sup>6</sup> The theoretical uncertainty is dominated by the hadronic contributions, particularly by the hadronic vacuum polarization (HVP) term, followed by the hadronic light by light (HLbL). The theoretical uncertainty is dominated by the contribution from the leading order HVP term, as summarized in Table 1. The key ingredient in the SM theoretical prediction for  $a_\mu$  is the critically compiled comprehensive data set on  $\sigma(e^+ + e^- \rightarrow \text{hadrons}) = \sigma_{\text{had}}(s)$  cross sections, that are subjected to a dispersion-relation integral transformation (based on the optical theorem and analyticity) to arrive at the HVP contribution  $a_\mu^{\text{HVP}}$  (see ref. <sup>6</sup> for details). We note that the uncertainties assigned to the QED and weak interaction contributions are insignificant in comparison to those of the hadronic terms in  $a_\mu^{\text{SM}}$ .

Meanwhile, the experimental evaluations of  $a_\mu$  have been steadily progressing toward ever more precise results. The third and final muon  $g-2$  experiment,<sup>7</sup> in a series of measurements at CERN, achieved a precision of 10 ppm for both  $a_{\mu+}$  and  $a_{\mu-}$ , in good mutual agreement. CPT symmetry was assumed, and the results were combined to give a 7.3 ppm measurement, in agreement with theory. This result presented the first confirmation of the predicted 60 ppm contribution to  $a_\mu$  from hadronic vacuum polarization. CERN-III experiment [5] used a uniform-field storage ring (SR) and electric quadrupoles to provide vertical containment for the muons having the “magic” momentum of 3.1 GeV/c. At this momentum, the muon spin precession is not affected by the electric field from the focusing quadrupoles.

The experimental effort was continued at the Brookhaven National Lab (BNL) in USA, refining the CERN-III approach and introducing significant innovations. In a series of measurements, the BNL E821 experiment improved the CERN-III precision by over an order of magnitude, to 0.7 ppm for both  $a_{\mu+}$  and  $a_{\mu-}$ .<sup>8</sup> It is at this point, historically, that appreciable differences emerged between the experimental and SM theoretical evaluations of  $a_\mu$ , as seen in Figure 2(a). The discrepancy,  $\sim 3\sigma$ , was compelling in motivating the formation of an expanded collaboration to perform a new round of measurements, improving further on the CERN-BNL technique, this time at Fermilab (experiment FNAL E989), where a more intense muon beam makes the desired improvement in precision feasible in principle.

Table 1: Top-level summary of the contributions to the SM value of  $a_\mu$  from each of the three fundamental interactions: electromagnetic (QED), weak, and hadronic (HVP and HLbL), along with their respective uncertainties, from the 2020 Muon  $g-2$  Theory Initiative White Paper <sup>6</sup> (further details are provided in the reference).

$a_\mu$ term	value ( $\times 10^{-11}$ )	uncertainty
QED	116,584,718.931	0.104
Weak	153.6	1.0
HVP	6,845	40
HLbL	92	18
Total SM	116,591,810	43

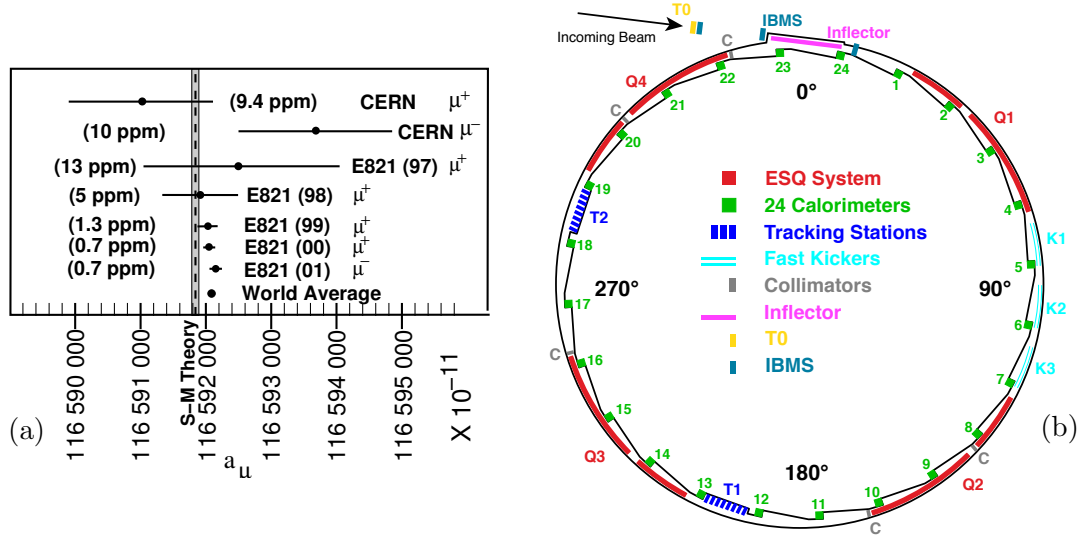


Figure 2 – (a) Evolution of the measured values for  $a_\mu$  in experiments at CERN and BNL, compared to the SM prediction, as of 2006, the time of the final BNL E821 results. (b) Layout of the Fermilab E989 storage ring that shares its design and most components with BNL E821, though with critical additions and upgrades. ESQ denotes the electrostatic quadrupole beam focusing system comprising quadrupoles Q1–Q4, IBMS is the Injector beam monitoring system comprising scintillating fiber detectors, T0 is a thin plastic scintillation detector providing the time profile of arriving muon bunches, K1–K3 are three pulsed kicker plates needed to place the muon into a stable stored orbit, T1 and T2 are in-vacuo straw-tube tracking detectors, and, outside the vacuum, electromagnetic calorimeter stations, numbered 1–24, to detect the decay positrons.

## 2 The Fermilab E989 Muon $g - 2$ experiment

The goal of the Fermilab E989 Muon  $g - 2$  experiment is to achieve a four-fold improvement in precision of  $a_\mu$  compared to the BNL E821 final result, i.e., an overall uncertainty in  $a_\mu$  of 140 ppb, balanced between the statistical and systematic uncertainties at 100 ppb each. The realization of this goal has required that the collaboration upgrade and calibrate the E821 apparatus to a new, higher standard, and that a new muon beam line be designed and constructed at FNAL.

Major components of the BNL E821 apparatus were transported from BNL on Long Island, New York, to Fermilab, in Batavia, Illinois, most critically the bulky  $\sim 15$  m diameter superconducting muon storage ring, in a storied trip that involved helicopters, a barge voyage along the US east coast, through the Gulf of Mexico, up the Mississippi and tributaries, as well as special trucks. The apparatus was assembled and installed in the new MC-1 Hall of the Fermilab Muon Campus. Painstaking shimming and calibration of the storage ring magnetic field was carried out in 2015-16 bringing the field uniformity to within 50 ppm, a stricter tolerance than was achieved in E821. In parallel, new apparatus, such as the 24 electromagnetic shower calorimeters, new in-vacuo straw-tube tracking stations, a complement of beam detectors, etc., were prepared for the start of measurements. By 2018, the collaboration started taking first physics data, in Run-1. In all, 6 runs were completed by the end of physics data acquisition, all with  $\mu^+$  beam. To date, data from Runs 1, 2 and 3 have been analyzed, and the results published.<sup>9,10,11</sup> The analysis of Runs 4-6 is ongoing, and its conclusion is anticipated soon.

It is not feasible, given the format limitations, to provide in this space a detailed discussion of all critical aspects of the experimental method, calibrations, Monte Carlo simulations and analysis, that would reflect the rigor required to reach the reported precision. We, instead, point the reader to Ref. <sup>11</sup> and references cited therein, and focus on the basic principles of the measurement.

The complete breaking of chiral symmetry in the weak interaction forces the spin vector of a positron with maximum energy (at the very endpoint of the Michel spectrum) in the decay

$\mu^+ \rightarrow \bar{\nu}_\mu + e^+ + \nu_e$ , to be aligned with  $\vec{S}_\mu$ , the spin of the decaying  $\mu^+$ . If  $\vec{S}_\mu$  is aligned with  $\vec{p}_\mu$ , the muon momentum (3.1 GeV/c), the emitted  $e^+$  is highly boosted, by a Lorentz  $\gamma_e$  of 29.3. If  $\vec{S}_\mu$  and  $\vec{p}_\mu$  are anti-aligned, or misaligned,  $\gamma_e$  drops precipitously. Thus,  $E_e$  provides an excellent measure of the (mis)alignment of  $\vec{S}_\mu$  and  $\vec{p}_\mu$ . Classical electrodynamics shows that the difference between  $\omega_S$ , the spin precession frequency in an external magnetic field  $B$ , and  $\omega_C$ , cyclotron (momentum precession) frequency, is determined by  $a_\mu$  and  $B$

$$\vec{\omega}_a = \vec{\omega}_S - \vec{\omega}_C = -\frac{e}{m} \left[ a_\mu \vec{B} - \left( a_\mu - \frac{1}{\gamma^2 - 1} \right) \frac{\vec{\beta} \times \vec{E}}{c} \right] \xrightarrow{\gamma \rightarrow 29.3} -\frac{e}{m} a_\mu \vec{B}, \quad (1)$$

i.e., the anomalous muon precession frequency becomes independent of the electric field  $\vec{E}$  at the “magic” momentum of  $\gamma = 29.3$ . Under these special circumstances,  $a_\mu$  can be determined from two measurements, of  $\omega_a$  and  $B$ , where the latter can be expressed in terms of  $\omega_p$ , the precession frequency of a proton in  $\vec{B}$ . The precision goal of E989, however, leads to the requirement that a number of corrections be applied, not the least of which being that the measurement of  $\vec{B}$  be weighted by the muon beam intensity for all points of  $(x, y)$  sampled by the beam along the circumference of the muon SR.

The principal experimental inputs into determining  $a_\mu$  are illustrated in Figure 3 based on data subsets collected in Run-2 and Run-3. Figure 3(a) shows the “wobble” plot of measured  $\omega_a$  oscillations (inset) and the accompanying Fourier analysis. Residuals from a basic fit not including all relevant beam dynamics terms show pronounced peaks associated with the frequencies of the omitted processes, primarily various modes of betatron oscillations. Figure 3(b) depicts an azimuthally averaged map of magnetic field strength, weighted by the reconstructed muon beam particle distribution in the radial-vertical displacement plane. In spite of the impressive field homogeneity, well under 1 ppm level where the muons pass, the beam density weighting remains necessary, on top of continuous field monitoring and frequent periodic probe cross-calibrations.

The SR magnetic field is mapped every few days using a trolley instrumented with nuclear magnetic resonance (NMR) probes housing petroleum jelly. These probes are calibrated using a retractable water-based cylindrical probe. This enables the expression of the magnetic field in terms of the precession frequency of shielded protons in a spherical sample  $\omega'_p$ , for which the relation between precession frequency and magnetic field is precisely known. Changes in the field between trolley measurements are tracked using 378 fixed NMR probes embedded in the vacuum chamber walls above and below the muon storage volume. Dedicated instrumentation was in place to monitor transient effects induced by the pulsing of kickers and electrostatic quadrupoles. It is particularly worth noting that all aspects of the data analysis were carried

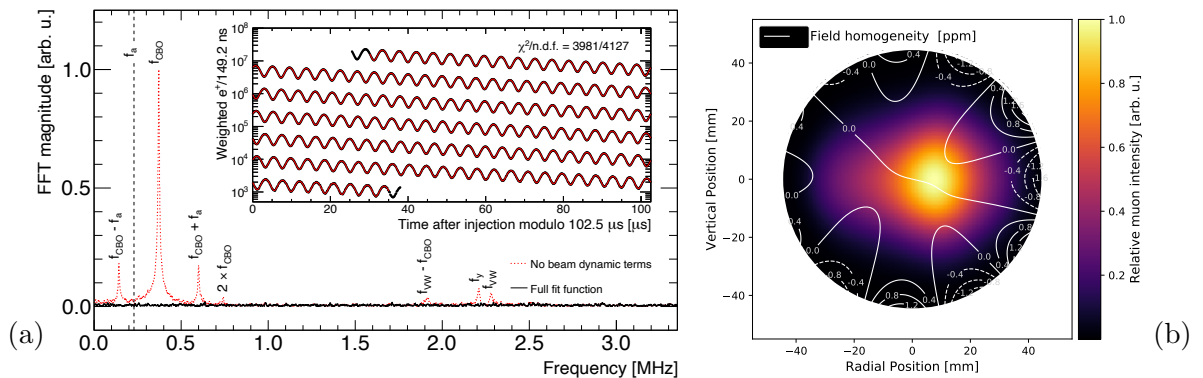


Figure 3 – (a) Fourier transform of the residuals from a basic fit not including three beam dynamics parameters (red dashed line), and from the full fit (black line). The peaks correspond to the missing betatron frequencies and muon losses. Data are from the Run-3a data set. Inset: corresponding asymmetry-weighted  $e^+$  time spectrum (black line) with the full fit function (red line) overlaid. (b) Azimuthally averaged magnetic field contours overlaid on the time- and azimuthally averaged muon distribution for the Run-3b data set. For more details see Refs.<sup>10,11</sup>

out in parallel by several groups independently. For example, the  $\omega_a$  “wiggle” plot analysis for Run-2 and Run-3 data was done by seven groups using independent analysis routines. Further, all E989 analysis is doubly blinded, with unblinding taking place in controlled phases.

The Run-1 unblinding took place in April 2021, and the unblinding for Runs 2 and 3 in July 2023. The results are summarized in Figure 4. Two observations readily stand out. First, the

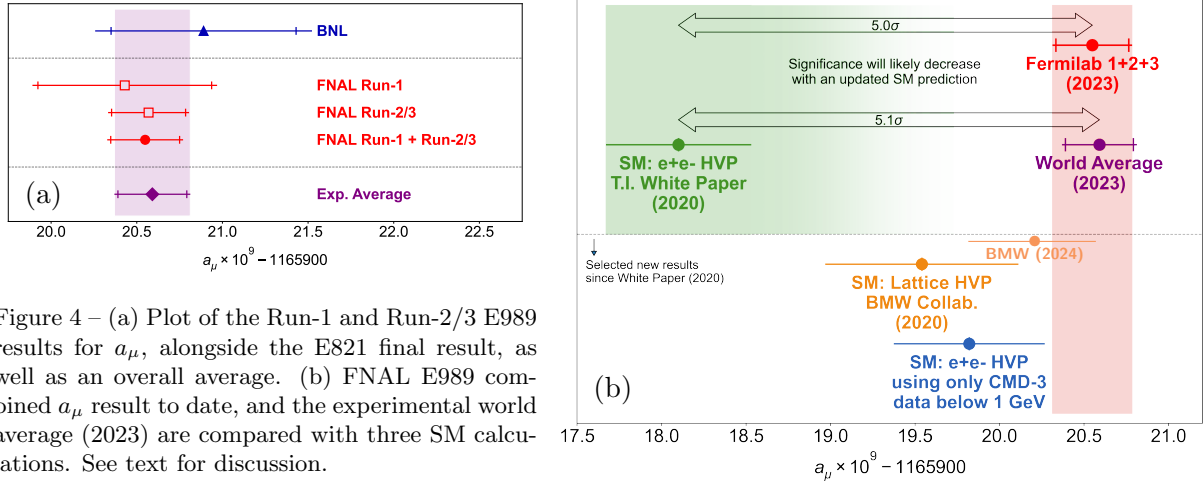


Figure 4 – (a) Plot of the Run-1 and Run-2/3 E989 results for  $a_\mu$ , alongside the E821 final result, as well as an overall average. (b) FNAL E989 combined  $a_\mu$  result to date, and the experimental world average (2023) are compared with three SM calculations. See text for discussion.

E989 results are remarkably internally consistent, and they are also consistent with the BNL E821 result [Figure 4(a)]. On the other hand, the discrepancy relative to the 2020 Muon  $g - 2$  TIWP result has only grown as new E989 results have become available, and currently exceeds  $5\sigma$ . Second, the experimental uncertainties are lower than the SM uncertainties in the 2020 TIWP.

However, the comparison with theoretical predictions is considerably muddled by the 2021 Lattice QCD result by the BMW collaboration<sup>12</sup>, which predicted a value for  $a_\mu$  less than  $2\sigma$  away from the experimental world average value. The 2021 BMW Lattice result is additionally reinforced by the 2023 experimental result for  $\sigma(e^+e^- \rightarrow \pi^+\pi^-)$ <sup>14</sup> for  $\sqrt{s} = 0.32 - 1$  GeV, which significantly differs from the world average  $\sigma_{\text{had}}(s)$  at comparable  $\sqrt{s}$ . Finally, the most recent update of their Lattice QCD calculation by the BMW collaboration<sup>13</sup>, marked as “BMW (2024)” in Figure 4, reduces their 2021 uncertainty by 40% and moves the central value closer to experiment, to within  $0.9\sigma$  of the current world average for  $a_\mu$ . Thus, there appears to be mounting evidence that the  $\sigma_{\text{had}}(s)$  data set underpinning the SM evaluation of  $a_\mu$  by the  $g - 2$  Theory Initiative needs to receive additional scrutiny.

Considerable experimental and theoretical effort will need to be expended in order to clarify the current inconsistencies between the dispersion relation based SM predictions of  $a_\mu^{\text{HVP}}$  and the Lattice QCD calculations of the same, resolve increasing inconsistencies apparent in the  $\sigma_{\text{had}}(s)$  data set, and to complete the E989 data analysis. All of this work is ongoing. In addition, interesting new experimental programs have been launched in order to provide independent measurements of  $a_\mu$  by different means and with radically different systematics.

Since 2009, an international collaboration has been pursuing a different measurement from the CERN/BNL/FNAL approach of storing muons at the “magic” momentum of  $3.1$  GeV/c. The JPARC Muon  $g - 2$  experiment starts with a cooled muon beam and accelerates it into a tighter storage ring with no need for electrostatic focusing.<sup>15</sup> The downside of this worthwhile project is that it will not be able to match or exceed that of E989, which limits it primarily to a consistency check. It is notable, though, that the JPARC experiment will also incorporate a measurement of the muon electric dipole moment with competitive sensitivity.

The MUonE experiment currently preparing to take its Phase-1 beam time in 2025, approaches the problem in a different way: it aims to determine the leading order term in  $a_\mu^{\text{HVP}}$  (the dominant source of the SM theoretical uncertainty) through precise measurement of muonic Bhabha scattering, with precision sufficient to address meaningfully the above inconsistencies.

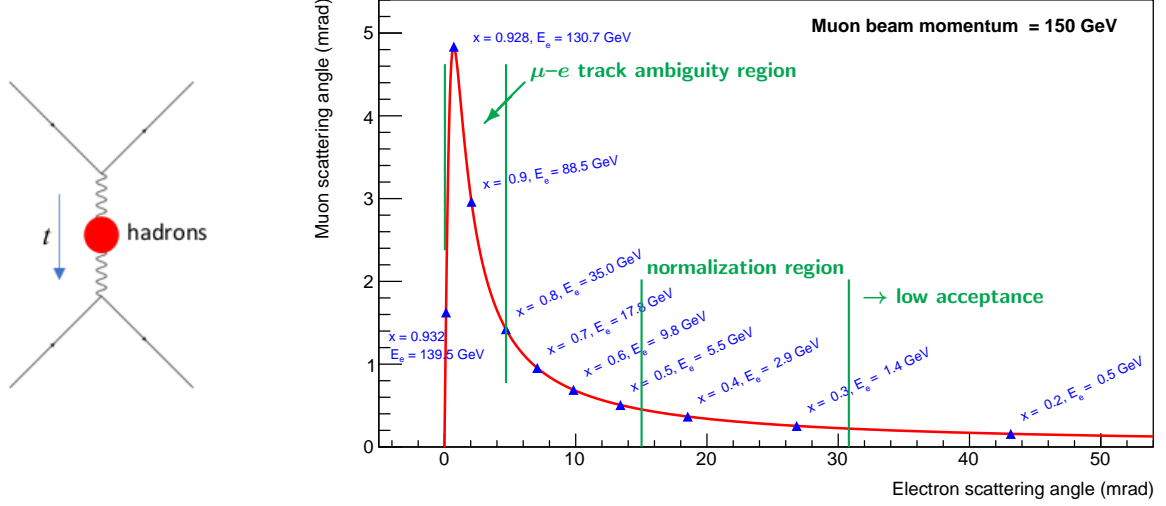


Figure 5 – The leading order Feynman diagram of interest in MUonE (left). The relation between the  $\mu$  and the  $e$  scattering angles for 150 GeV incident muon beam momentum (right). The blue triangles indicate the reference values of the variable  $x$  and the electron energy, while green lines indicate the approximate boundaries of the three kinematic regions of interest in the experiment.

### 3 The MUonE experiment at CERN

The MUonE collaboration, constituted in 2018, aims to complement the Muon  $g-2$  program by experimentally addressing the leading-order HVP contribution  $a_\mu^{\text{HLO}}$ , the largest source of theoretical uncertainty in  $a_\mu$ <sup>16</sup>. In light of the preceding discussion and results shown in Fig. 4(b), that decision appears prescient. Using the theoretical relationship discussed in Refs.<sup>17,18</sup>, MUonE will evaluate the hadronic contribution  $\Delta\alpha_{\text{had}}$  to the running of  $\alpha$ , the electromagnetic coupling, in a precise measurement of muon Bhabha scattering on atomic electrons using a 160 GeV muon beam in the M2 (North Area) beamline at CERN. MUonE’s focus is on the leading order (LO) hadronic contribution to  $a_\mu$  via the relation<sup>17</sup>

$$a_\mu^{\text{HLO}} = \frac{\alpha}{\pi} \int_0^1 dx (1-x) \Delta\alpha_{\text{had}}[t(x)], \quad t(x) = \frac{x^2 m_\mu^2}{x-1} < 0, \quad (2)$$

where  $m_\mu$  is the muon mass and  $\alpha$  is the fine-structure constant. The hadronic contribution to the running of the effective electromagnetic coupling,  $\Delta\alpha_{\text{had}}(t)$ , evaluated at the space-like squared four-momentum transfer  $t(x)$ , will be extracted from MUonE’s precise  $\mu$ - $e$  scattering measurements. The  $\mu$ - $e$  two-body angular correlation is shown in Fig. 5, along with the corresponding  $x$  and  $E_e$  values. The  $\Delta\alpha_{\text{had}}(t)$  term is strongest for  $\theta_{\mu,e} \lesssim 5$  mrad, where the two cannot be unambiguously separated on the basis of angle alone.

While there are considerable theoretical advantages over the dispersion approach through time-like processes:  $e^+e^- \rightarrow \text{hadrons}$ , such as absence of resonances, this space-like scattering approach presents formidable experimental challenges and requires highly accurate simulations.

MUonE requires control of systematics at  $\sim 10$  ppm level in order for the subtraction of the leptonic, top-quark, and weak contributions to  $\Delta\alpha$  to be effective. This calls for a light (Be) target segmented into 40 slices, each followed by a  $\sim 1$  m long tracking station; an electromagnetic calorimeter (ECAL) and  $\mu$  detector are at the end of apparatus<sup>16</sup>. MUonE aims to achieve  $\sim 0.3\%$  statistical, and  $< 0.5\%$  overall relative uncertainty in  $a_\mu^{\text{HLO}}$  in  $\sim 2$  years of data taking. Layout of the full MUonE apparatus is sketched in Fig. 6, as well as the Phase-1 layout, to be used in the 2025 beam period. A closer look at the make-up of a tracker station and a look at the ECAL  $5 \times 5$  PbWO<sub>4</sub> (PWO) calorimeter are found in Figure 7. At the heart of the experiment are the 2S tracking modules composed of two single-sided Si microstrip detectors developed for CMS.<sup>20</sup> The PWO single crystals were also originally used in the CMS ECAL.<sup>21,22</sup> For MUonE,



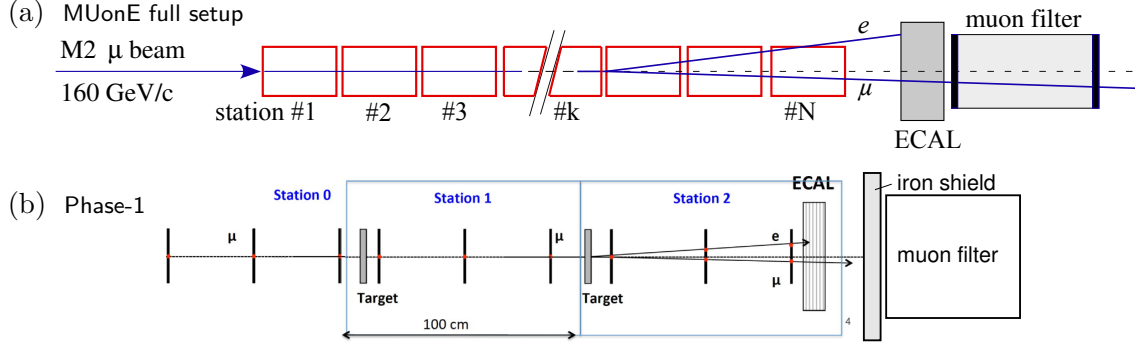


Figure 6 – Layout sketches (not to scale) for: (a) the final MUonE apparatus with  $N = 40$  tracking stations, and (b) the Phase-1 measurements approved for 2025 in the M2 beamline.

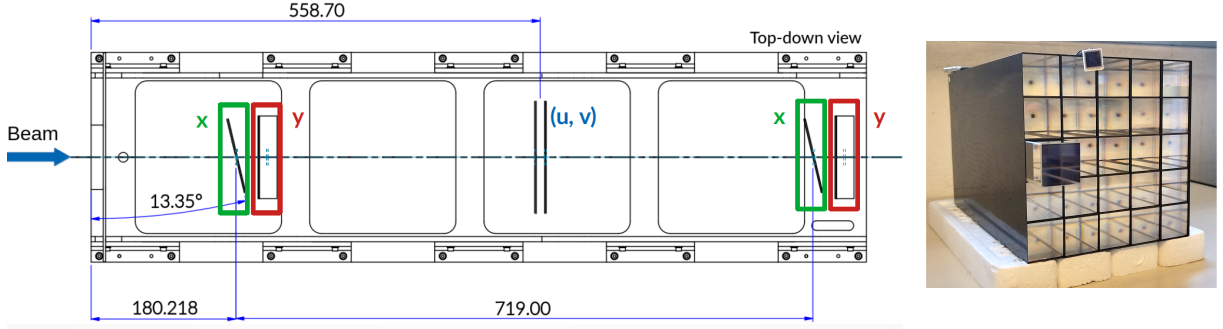


Figure 7 – (a) An engineering drawing of a tracking station, showing how the  $x$  and  $y$  modules are tilted. The graphite target is on the left, with its upstream face at the edge of the diagram. All dimensions are in mm. (b) Photograph of the 25 PWO crystals placed inside the carbon fiber alveolar matrix (downstream view). Resting on the top of the structure is a single  $10 \times 10 \text{ mm}^2$  APD, used to detect the scintillation light.

the ECAL scintillation light is read out by APDs, while the front-end electronics is based on the multi-gain preamplifier (MGPA) chips<sup>23</sup> developed for the CMS ECAL. Instrument goals include energy resolution  $\sigma(E)/E \sim 1\%$  above 100 GeV and position resolution of  $\lesssim 1 \text{ mm}$  for the reconstructed electron impact point. MUonE has carried out a number of beam tests with individual components of the current apparatus, as well as a complement of two or three tracking stations and ECAL. A few representative preliminary results of these measurements are depicted in Figure 8. As evinced in the figure, the key components of the MUonE apparatus have met the basic requirements, and demonstrated the experimental proof of principle.

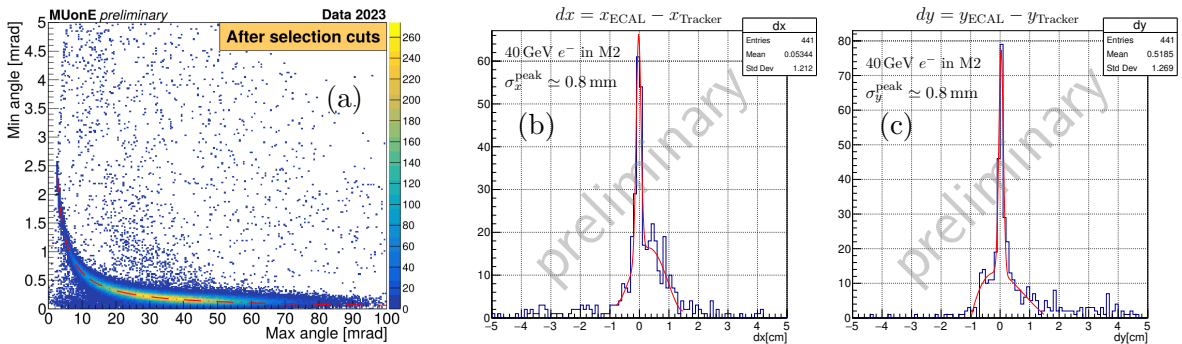


Figure 8 – Preliminary results from 2023 test beam data set. (a)  $\theta_{\min}$  vs.  $\theta_{\max}$  distribution of elastic scattering candidates after the preliminary event selection. The red dashed line represents the expected elasticity curve for a 160 GeV muon beam. (b) and (c)  $x$  and  $y$  spatial coordinate differences between the projected Tracker impact points on the ECAL front face, and the reconstructed electromagnetic shower centers, for synchronised Tracker-ECAL events (40 GeV  $e^-$  beam). The near-Gaussian peaks, with  $\sigma_{x,y} \simeq 0.8 \text{ mm}$ , are consistent with Monte Carlo simulations of the same setup.

## 4 Conclusions: prospects for $a_\mu$ and hadronic vacuum polarization

In the coming year or two, the Fermilab E989 collaboration will unblind and publish the results of analysis of the remaining three runs, Run-4 through 6, or about 2/3 of the total data. A significant improvement in precision is expected over their Run-1/3 results, which have already exceeded the overall goal for the systematic uncertainty. Evidence appears to be increasing for a real discrepancy between the Lattice QCD and dispersion-relation determinations of  $a_\mu^{\text{HLO}}$ . In the near future, strong ongoing efforts on the theoretical side, as well as the new experiments: MUonE at CERN and Muon  $g - 2$ /EDM experiment at J-PARC, will provide much needed fresh experimental evidence with radically different methods and systematics than the previous experiments.

## Acknowledgments

This work has been supported by grants from the US National Science Foundation, most recently PHY-2209484.

## References

1. P.A.M. Dirac, *Proc. R. Soc. A* **118**, 351 (1928).
2. J.S. Schwinger, *Phys. Rev.* **73**, 416 (1948).
3. P. Kusch and H.M. Foley, *Phys. Rev.* **74**, 250 (1948).
4. R.L. Garwin, D.P. Hutchinson, S. Penman, and G. Shapiro, *Phys. Rev.* **118**, 271 (1960).
5. F. Jegerlehner, *The anomalous magnetic moment of the muon*, 2nd ed., Springer Tracts in Mod. Phys. **274** (2017).
6. T. Aoyama *et al.*, *Phys. Rept.* **887**, 1 (2020).
7. J. Bailey *et al.*, *Nucl. Phys. B* **150**, 1 (1979).
8. G.W. Bennett *et al.*, *Phys. Rev. D* **73**, 072003 (2006).
9. B. Abi *et al.*, *Phys. Rev. Lett.* **126**, 141801 (2021).
10. D.P. Aguillard *et al.*, *Phys. Rev. Lett.* **131**, 161802 (2023).
11. D.P. Aguillard *et al.*, *Phys. Rev. D* **110**, 032009 (2024).
12. Sz. Borsanyi *et al.*, *Nature (London)*, **593**, 51 (2021).
13. A. Boccaletti *et al.*, arXiv 2407.10913 (2024).
14. F. Ignatov *et al.*, (CMD-3 collaboration), *Phys. Rev. D* **109**, 112002 (2024).
15. M. Abe *et al.*, *PTEP* **2019**, 053C02, arXiv:1901.03047 (2019).
16. G. Abbiendi *et al.* (MUonE Collaboration), CERN report: CERN-SPSC-2019-026/SPSC-I-252 (June 2019) <https://cds.cern.ch/record/2677471>.
17. C.M. Carloni Calame, M. Passera, L. Trentadue and G. Venanzoni, *Phys. Lett. B* **746**, 325 (2015).
18. E. de Rafael, *Phys. Rev. D* **102**, 056025 (2020).
19. G. Abbiendi *et al.*, (MUonE Collaboration), CERN-SPSC-2024-015 (August 2024), 54 pages, available from: <https://cds.cern.ch/record/2896293>.
20. CMS Collaboration, CERN report: CERN-LHCC-2017-009, CMS-TDR-014, (2017).
21. S. Chatrchyan *et al.*, *JINST* **3**, S08004 (2008).
22. S. Chatrchyan *et al.*, CERN report: CMS-EGM-11-001, CERN-PH-EP-2013-097 and arXiv:1306.2016 (2013).
23. M. Raymond, G. Hall, J. Crooks and M. French, *IEEE Trans. Nucl. Sci.* **52**, 756 (2005).